Synthesis, Reduction Chemistry, and Spectroscopic and Computational Studies of Isomeric Quinolinecarboxaldehyde Triosmium Clusters

Edward Rosenberg* and Dalia Rokhsana

Department of Chemistry, University of Montana, Missoula, Montana 59812

Carlo Nervi, Roberto Gobetto, Luciano Milone, and Alessandra Viale

Dipartimento di Chimica IFM, Università di Torino, 10125 Torino, Italy

Jan Fiedler

J. Heyrovský Institute of Physical Chemistry, Academy of Sciences of the Czech Republic, 18223 Prague, Czech Republic

Maria Alexandrovna Botavina

N. D. Zelinsky Institute of Physical Chemistry, Russian Academy of Science, Leninsky Prospect 47, 117913 Moscow, Russia

Received August 5, 2003

The quinoline derivatives $Os_3(CO)_n(\mu_m\text{-}\eta^2\text{-L-H})(\mu\text{-H})$ (L = quinoline-4-carboxaldehyde, n = 10, m = 2, **4**; n = 9, N−C(8) bound, m = 3, **5**; n = 10, N−C(2) bound, m = 2, **6**; L = quinoline-3-carboxaldehyde, n = 9, N−C(8) bound, m = 3, **7**) are obtained by the reaction of $Os_3(CO)_{10}(CH_3CN)_2$ with the quinoline-3-carboxaldehyde or -4-carboxaldehyde ligand followed by photochemical decarbonylation in the case of **5** and **7**. The quinoline-4-carboxaldehyde clusters and the free ligand all show reversible 1e$^-$ reductions, but the electron-deficient **5** shows two separate reversible 1e$^-$ reductions, the first at much less negative potential than for the previously investigated $Os_3(CO)_9(\mu_3\text{-}\eta^2\text{-L-H})(\mu\text{-H})$ (L = phenanthridine, **1**; L = 5,6-benzoquinoline, **2**), while the free ligand is reduced at a more negative potential than any of the clusters. The spectroscopic properties of the clusters upon electrochemical and chemical reduction have been investigated, and in the case of **4** selective line broadening of its ^{1}H NMR resonances is observed. Infrared spectrophotoelectrochemistry reveals that the CO stretching modes are shifted to lower frequencies, as expected. The pattern of unpaired spin densities in the reduced clusters predicted from the DFT calculations correlates with the observed selective line broadening, and EPR measurements confirm the formation of the radical anions at g values similar to those observed for pure organic radical anions.

Introduction

Metal complexes with biomedically important benzo heterocycles have attracted considerable attention.[1−6] Some of the research on benzo heterocycle metal complexes has explored their interaction with biomacromolecules, and these complexes have been used as DNA markers or intercalating agents.[4] Polymetallic complexes are receiving much attention because the polymetallic core allows direct extraction of the phase information from single-crystal X-ray diffraction experiments and in some cases this information can be directly located by electron microscopy when the complex binds with the biomacromolecule.[7] In the particular case of triosmium clusters, positive or negative charges have been placed on the metal core and on the ring to impart water solubility.[8,9] The resulting charged clusters are stable in water over a wide range of pH, owing to the air and thermal stability of the triosmium framework. The synthesis of complexes with like charges on both the ring and the metal prevents aggregation of these clusters in aqueous solution, allowing for more specific interactions and sharper spectroscopic signals.[9] The

* Corresponding author.

(1) Kraatz, H. B.; Lusztyk, J.; Enright, G. D. *Inorg. Chem.* **1997**, *36*, 2400.
(2) Grotjahn, D. B.; Joubran, C.; Combs, D.; Brune, D. C. *J. Am. Chem. Soc.* **1998**, *120*, 11814.
(3) Grofti, A.; Michele, S.; Jaouen, G.; McGlinchey, M. J.; Bennouna, A.; Mousser, A. *Organometallics* **1996**, *15*, 142.
(4) Jaouen, G.; Vessieres, A.; Butler, I. S. *Acc. Chem. Res.* **1993**, *26*, 361.
(5) Barton, J. K. *Chem. Rev.* **1999**, *99*, 2777.
(6) Burrows, C. J.; Muller, J. G. *Chem. Rev.* **1998**, *98*, 1109.
(7) Furuya, F. R.; Miller, L. L.; Hainfeild, J. F.; Christopher, W. C.; Keny, P. W. *J. Am. Chem. Soc.* **1988**, *110*, 641.
(8) Arcia, E.; Rosenberg, E.; Kolwaite, D. S.; Hardcastle, K. I.; Ciurash, J.; Duque, R.; Gobetto, R.; Milone, L.; Osella, D.; Botta, M.; Dastrú, W.; Viale, A.; Fiedler, J. *Organometallics* **1998**, *17*, 415.
(9) Rosenberg, E.; Spada, F.; Sugden, K.; Martin, B.; Milone, L.; Gobetto, R.; Viale, A.; Fiedler, J. *J. Organomet. Chem.* **2003**, *668(1−2)*, 51.

10.1021/om030564m CCC: $27.50
Publication on Web 12/13/2003

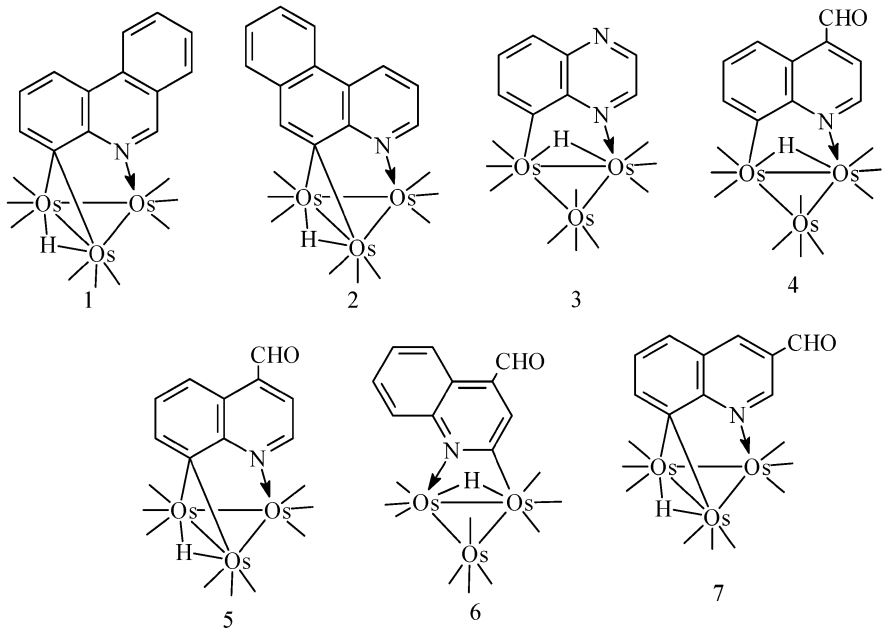

Figure 1. Structures of the osmium benzoheterocycle triosmium clusters, which show reversible reduction potentials.

clusters synthesized for this purpose so far possess carbonyl and hydride ligands that have infrared and NMR signals in regions where proteins and polynucleotides are silent.[10−12]

In light of these advantages, we have recently developed procedures for the synthesis of the electron-deficient complexes of biomedically important benzo heterocycles with triosmium clusters of the general formula $Os_3(CO)_9(\mu_3\text{-}\eta^2\text{-L-H})(\mu\text{-H})$ (L = benzo heterocycle) (Scheme 1).[8−14] For example, decarbonylation of the N−C(8) activated $Os_3(CO)_{10}(\mu\text{-}\eta^2\text{-L})(\mu\text{-H})$ cluster (which is the major product of the reaction of quinoline with $Os_3(CO)_{10}(CH_3CN)_2$, the other product being the N−C(2) activated $Os_3(CO)_{10}(\mu\text{-}\eta^2\text{-L})(\mu\text{-H})$) gives the electron-deficient $Os_3(CO)_9(\mu_3\text{-}\eta^2\text{-L-H})(\mu\text{-H})$ (L = quinoline; Scheme 1). The electrochemical properties of these complexes are of interest not only because they will elucidate the electron-acceptor properties of these clusters but also because their study will allow us to understand how modification of the benzo heterocycle ring can alter these properties.

Scheme 1

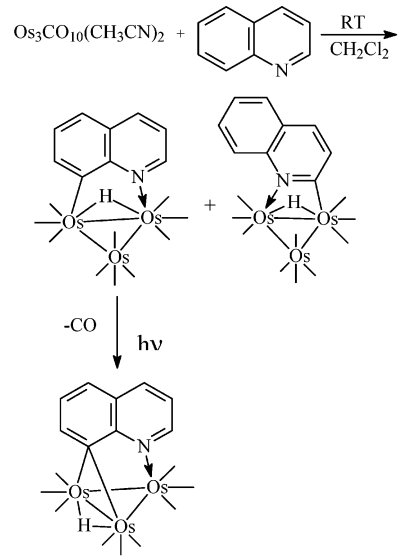

Indeed, we have previously reported that the structure of the organic ligand can have a profound influence on the electron-acceptor properties of benzo heterocycle triosmium clusters, both in terms of reduction potential and in terms of the stability of the resulting radical anions.[14,15] Thus, we have found that the electron-deficient clusters $Os_3(CO)_9(\mu_3\text{-}\eta^2\text{-L-H})(\mu\text{-H})$ (L= phenanthridine, **1**; L = 5,6-benzoquinoline, **2**) and also electron-precise $Os_3(CO)_{10}(\mu\text{-}\eta^2\text{-L-H})(\mu\text{-H})$ (L = quinoxaline, **3**) (Figure 1) undergo reversible one-electron reductions while quinoline itself undergoes rapid reaction after reduction leading to decomposition. The reduction processes in **1**−**3** are associated with intense color changes, making these compounds potential candidates for components in optical materials.[16] The formation of stable radical anions by these clusters may provide novel regioselective electrophilic substitution or addition to the benzo heterocyclic ring, at the positions of highest spin density, as a result of the cluster's influence on the spin distribution patterns.[17] Density functional theory calculations have been shown to provide a detailed understanding of how a trimetallic core affects the spin density distribution in the radical anions resulting from the reduction of **1**−**3**.[18,19] With these factors in mind,

(10) Abedin, M. J.; Bergman, B.; Holmquist, R.; Smith, R.; Rosenberg, E.; Ciurash, J.; Hardcastle, K. I.; Roe, J.; Vazquez, V.; Roe, C.; Kabir, S. E.; Roy, B.; Alam, S.; Azam, K. A. *Coord. Chem. Rev.* **1999**, *190−192*, 975.

(11) Bergman, B.; Holmquist, R.; Smith, R.; Rosenberg, E.; Hardcastle, K. I.; Visi, M.; Ciurash, J. *J. Am. Chem. Soc.* **1998**, *120*, 12818.

(12) Smith, R.; Rosenberg, E.; Hardcastle, K. I.; Vazquez, V.; Roh, J. *Organometallics* **1999**, *18*, 3519.

(13) Bar Din, A. V.; Bergman, B.; Rosenberg, E.; Smith, R.; Dastrú, W.; Gobetto, R.; Milone, L.; Viale, A. *Polyhedron* **1998**, *17*, 2975.

(14) Rosenberg, E.; Abedin, M. J.; Rokhsana, D.; Osella, D.; Milone, L.; Nervi, N.; Fiedler, J. *Inorg. Chim. Acta* **2000**, *300−302*, 769.

(15) Rosenberg, E.; Abedin, M. J.; Rokhsana, D.; Viale, A.; Dastrú, W.; Gobetto, R.; Milone, L. *Inorg. Chim. Acta* **2002**, *334*, 343.

(16) Spangler, C. W. *J. Mater. Chem.* **1999**, *9*, 2013.

(17) Salzmann, R.; Ziegler, C. J.; Godbout, N.; McMahon, M. T.; Suslick, K. S.; Oldfield, E. *J. Am. Chem. Soc.* **1998**, *120*, 11323.

we thought it would be interesting to explore the effect of modifying the previously reported unstable radical anion of quinoline with a substituent that is a good electron acceptor and to elucidate the impact of putting this modifying group in two different positions. We report here the synthesis and electrochemical and chemical reduction as well as the spectroscopic and computational study of the clusters resulting from the reaction of $Os_3(CO)_{10}(CH_3CN)_2$ with quinoline-3-carboxaldehyde and -4-carboxaldehyde.

Results

A. Synthesis of the Quinoline-3-carboxaldehyde and -4-carboxaldehyde Clusters. The synthesis of the target clusters proceeds in a manner analogous to Scheme 1. The deep red compound $Os_3(CO)_{10}(\mu\text{-}\eta^2\text{-L-H})(\mu\text{-H})$ (**4**; L = quinoline-4-carboxaldehyde) is obtained in moderate yield (33% based on $Os_3(CO)_{12}$) and is quantitatively decarbonylated to $Os_3(CO)_9(\mu_3\text{-}\eta^2\text{-L-H})(\mu\text{-H})$ (**5**; L = quinoline-4-carboxaldehyde) on photolysis to give the latter in 31% overall yield. Compound **4** is, in fact, somewhat light sensitive and slowly converts to **5** on standing in ambient light. The N−C(2) bound cluster $Os_3(CO)_{10}(\mu\text{-}\eta^2\text{-L-H})(\mu\text{-H})$ (**6**; L = quinoline-4-carboxaldehyde) is also obtained in 12% yield. The electron-deficient green cluster $Os_3(CO)_9(\mu_3\text{-}\eta^2\text{-L-H})(\mu\text{-H})$ (**7**; L = quinoline-3-carboxaldehyde) is obtained in 30% overall yield (based on $Os_3(CO)_{12}$) in a manner analogous to Scheme 1. The intermediate decacarbonyl was isolated and converted directly to **7** without spectroscopic characterization. In the case of quinoline-3-carboxaldehyde the analogue of **6** is also obtained in 11.4% yield and has been characterized by ^{1}H NMR and IR spectroscopy.

B. Electrochemistry of 4−7. In our previous studies, we reported that compounds **1** and **2** showed reversible one-electron reductions at −1.52 and −1.44 V vs $FeCp_2/FeCp_2^+$ in CH_2Cl_2.[14] Spectroscopic investigations of the resulting radical anions revealed a regioselective distribution of spin density that could be understood with the aid of DFT calculations.[19] The ^{1}H NMR of these complexes revealed selective line broadening at the 2-, 7-, and 9-positions for $\mathbf{1}^-$ and at the 6-, 8-, and 9-positions of the heterocyclic ring for $\mathbf{2}^-$. This selective line broadening could be understood in terms of rapid electron transfer between the radical and its unreduced counterpart in partially reduced solutions of **1.** The orbital composition of the LUMO and the spin density distribution obtained from the DFT calculations nicely rationalized the regioselectivity of the observed line broadening.[19] However, cyclic voltammetry of **5** shows two reversible 1e$^-$ reductions at half-wave potentials of −1.12 and −1.68 V vs $FeCp_2/FeCp_2^+$ (Figure 2, top), whereas the electron-precise **4** and **6** show single 1e$^-$ reductions at significantly more negative potentials, −1.54 and −1.66 V, respectively (Table 1). In the case of the quinoline-4-carboxaldehyde free ligand, a reversible 1e$^-$ reduction is observed at −1.86 V (Table 1). The charge consumption of 1 F/mol was confirmed by controlled coulometry at the half-wave potential for **5** (Figure 2, bottom). This was also confirmed for compounds **4**, **6** and the free ligand.

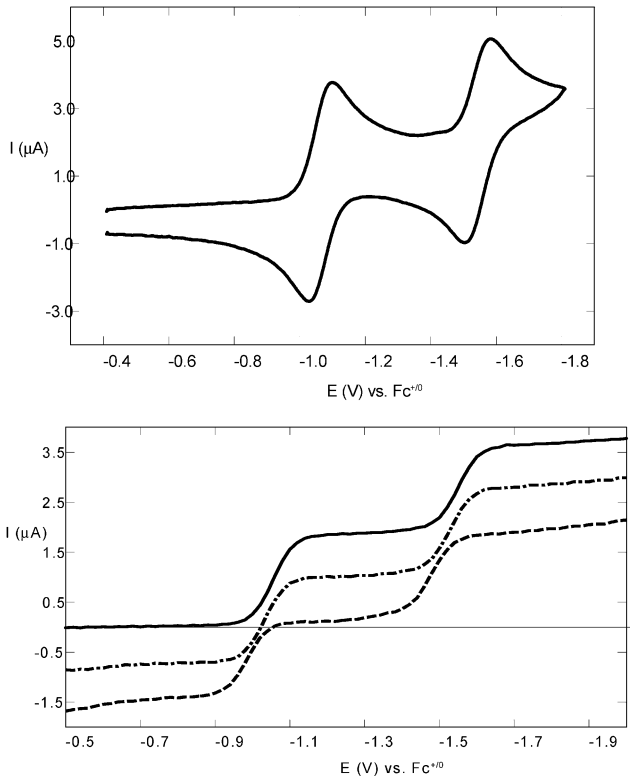

Figure 2. (Top) Cyclic voltammogram of **5** in CH_2Cl_2 at a Pt electrode, 200 mV/s scan rate. (Bottom) Polarographic monitoring of changes during controlled-potential coulometry at −1.2 V, with 1.0 mM of **5** in CH_2Cl_2/0.1 M Bu_4NPF_6 (—), reduced by 0.5 F/mol (— · —), and reduced by 1.0 F/mol (- - -).

Table 1. Reversible Reduction Potentials of Compounds 4−7[a]

compd	$E°_{1/2}$[a] (V)
5	−1.17 (E_{REV}, 1e$^-$)
	−1.68 (E_{REV}, 1e$^-$)
4	−1.54 (E_{REV}, 1e$^-$)
6	−1.66 (E_{REV}, 1e$^-$)
quninoline-4-carboxaldehyde (free ligand)	−1.86 (E_{REV}, 1e$^-$)
7	−1.28 (E_{IRR}, 1e$^-$)

[a] Relative to Fc/Fc^+ in CH_2Cl_2.

From the observed reduction potentials, one can conclude that the ability to accept an electron is strongly dependent on the structure of the clusters. In general, we find that the electron-deficient clusters show lower reduction potentials than their electron-precise precursors.[14] Here the use of a ligand that already had a reversible 1e$^-$ reduction results in the creation of a second reversible wave, perhaps involving a cluster ligand interaction. In addition, it appears that the N−C(8) bonding mode provides better delocalization of the added electron than the N−C(2) bonding mode, since the reduction potential of **4** is considerably less than that of **6**.

In the previously reported quinoline series we found that electron-donating substituents in the 5-position of the ring shifted the reduction potentials of the electron-deficient clusters toward more negative values (e. g. 5-aminoquinoline $\Delta E_{1/2} = -0.12$ V).[14] In the case of **4**−**6**, the electron-withdrawing carboxaldehyde group located

(18) Holy, N. L. *Chem. Rev.* **1974**, *74*, 243.
(19) Rosenberg, E.; Rokhsana, D.; Nervi, N.; Fiedler, J.; Gobetto, R.; Milone, L.; Viale, A. *Chem. Eur. J.*, in press.

in the 4-position serves as an excellent electron acceptor, shifting the potential to less negative values relative to the parent quinoline complex (−1.38 V vs $FeCp_2/FeCp_2^+$) and stabilizing the resulting radical anion sufficiently to make the reduction chemically reversible; the unsubstituted quinoline did not undergo a chemically reversible process. Surprisingly, even though compound **7** shows a reduction wave at much lower potential (−1.28 V vs $FeCp_2/FeCp_2^+$) than the unsubstituted quinoline, this process was not reversible at all. This indicates that the position of the substituent group also has a significant impact on the stability of the radical anion found after 1e⁻ reduction. The reduction potential and the stability of the resulting radical anion are probably related to the LUMO energy of the complexes (vide infra).

C. Chemical Reductions and Spectroscopic Investigations of the Resulting Radical Anions. The electrochemical reduction of **5** was followed by FTIR using an optically transparent thin-layer electrochemical (OTTLE) cell.[20] This reveals a fully reversible reduction/oxidation cycle during which the carbonyl stretching frequencies are shifted to lower frequencies (from 2079 s, 2050 s, 1992 vs, 1982 sh, 1955 m, 1944 m to 2058 s, 2027 vs, 2001 vs, 1969 vs, 1955 s, 1933 s, 1918 sh) without significant change in the overall pattern of the spectrum (Figure 3). The most significant changes are for the carbonyl stretching frequencies of the aldehyde substituent on the quinoline ring at 1711 cm^{-1}, which disappears upon reduction while three new bands appear at 1602, 1565, and 1525 cm^{-1}. The strongest of these bands is at 1602 cm^{-1}, and it tempting to assign this band to a carbon−oxygen stretch of reduced bond order. However, it is not possible to define which of these bands is the reduced C−O stretch without the aid of isotopic substitution. All three bands disappear during reoxidation, and the original band at 1711 cm^{-1} is restored. Spectral changes with rather good isosbestic points were observed after the second electron reduction, and only one weak band was found at 1527 cm^{-1}, the other two bands at 1602 and 1565 cm^{-1} having disappeared. This suggests that the cluster structure remains unchanged during the experiment conducted in the OTTLE cell but the environment of the aldehyde group is significantly impacted.

Using the known reduction potential for cobaltocene in CH_2Cl_2, we can calculate the equilibrium constants for the reduction of **4**−**6** (Table 2).[21] This predicts that **5** will be fully reduced by cobaltocene, while **4** and **6** will be only partially reduced. Spectroscopic investigations bear this out. Thus, the ^{1}H NMR studies of **5** reveal that the first electron reduction, induced by electrochemical means or with cobaltocene, results in a fully reduced species where all the resonances are broadened into the baseline. EPR spectroscopy of these solutions shows a reasonably narrow EPR signal at a *g* value typical for an organic radical (*g* value 1.999). The addition of excess cobaltocene leads to the appearance of relatively sharp aromatic and hydride resonances at values different from those of **5**. This is likely due to the formation of the diamagnetic dianion in solution.

(20) Krejcik, M.; Danek, M.; Hartl, F. *J. Electroanal. Chem. Interfacial Electrochem.* **1991**, *317*, 179.
(21) Connelly, N. G.; Geiger, W. E. *Chem. Rev.* **1996**, *96*, 877.

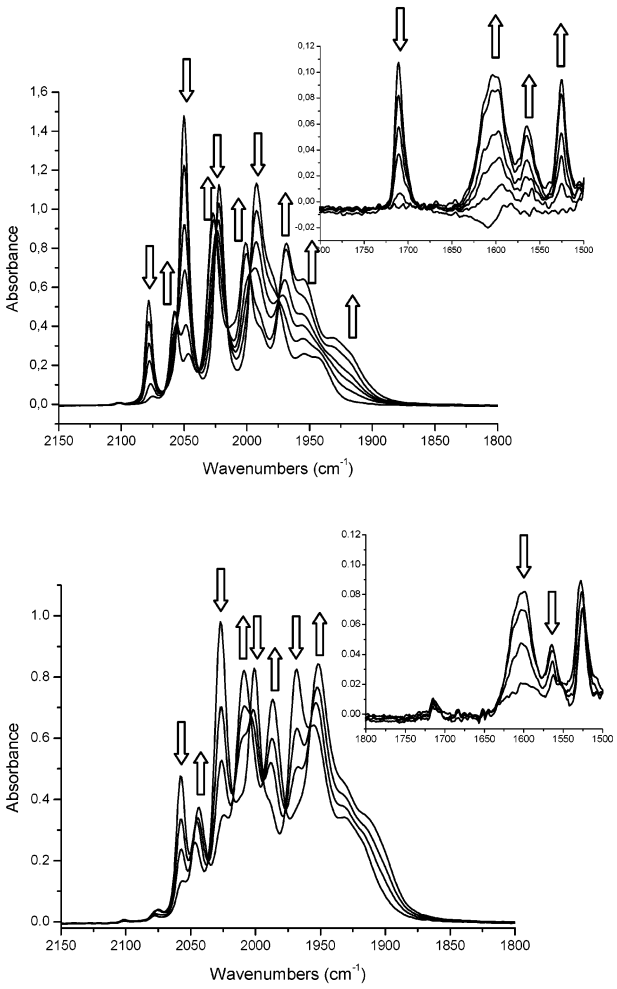

Figure 3. Time-resolved IR spectroelectrochemical response of **5** in the CO stretching region during exhaustive electrolysis of (top) the first electron reduction of **5** at $E = -0.8$ V and (bottom) the second electron reduction of **5** at $E = -1.3$ V.

Table 2. Equilibrium Constants for the Reactions of 4−6 with Cobaltocene

compd	$E°_{cell}$ (V)	K_{eq}[a]
5 → **5**⁻	0.21	3.72×10^3
5⁻ → **5**²⁻	0.77	1.0×10^{13}
4 → **4**⁻	−0.21	2.4×10^{-4}
6 → **6**⁻	−0.33	2.5×10^{-6}

[a] Reduction potential of Cp_2Co −1.33 V relative to Fc/Fc^+ from: Connelly, N. G.; Geiger, W. E. *Chem. Rev.* **1996**, *96*, 877.

The ^{1}H NMR resonances of **5** shifted from δ 9.66 (dd, H(2) & H(5)), 8.74 (d, H(7)), 7.51 (d, H(3)), 7.38 (dd, H(6)), and −12.23 (s, hydride) to δ 9.66 (d, H(2)), 9.18 (d, H(5)), 8.60 (d, H(7)), 7.34 (d, H(3)), 7.19 (dd, H(6)), and −12.18 (s, hydride). Note that no aldehyde resonance was found for the diamagnetic dianion after the second 1e⁻ reduction. There were several singlet resonances between δ 4 and 5, but they could not be differentiated from the cobaltocenium peaks in this same region. The largest shift in the ^{1}H NMR is observed for the protons resonating at δ 9.66 (H(2) and H(5); assignments are based on COSY and NOESY experiments). After the 2e⁻ reduction, one of the two protons is shifted from δ 9.66 to 9.18. No EPR signal is observed for **5** reduced with excess cobaltocene, as

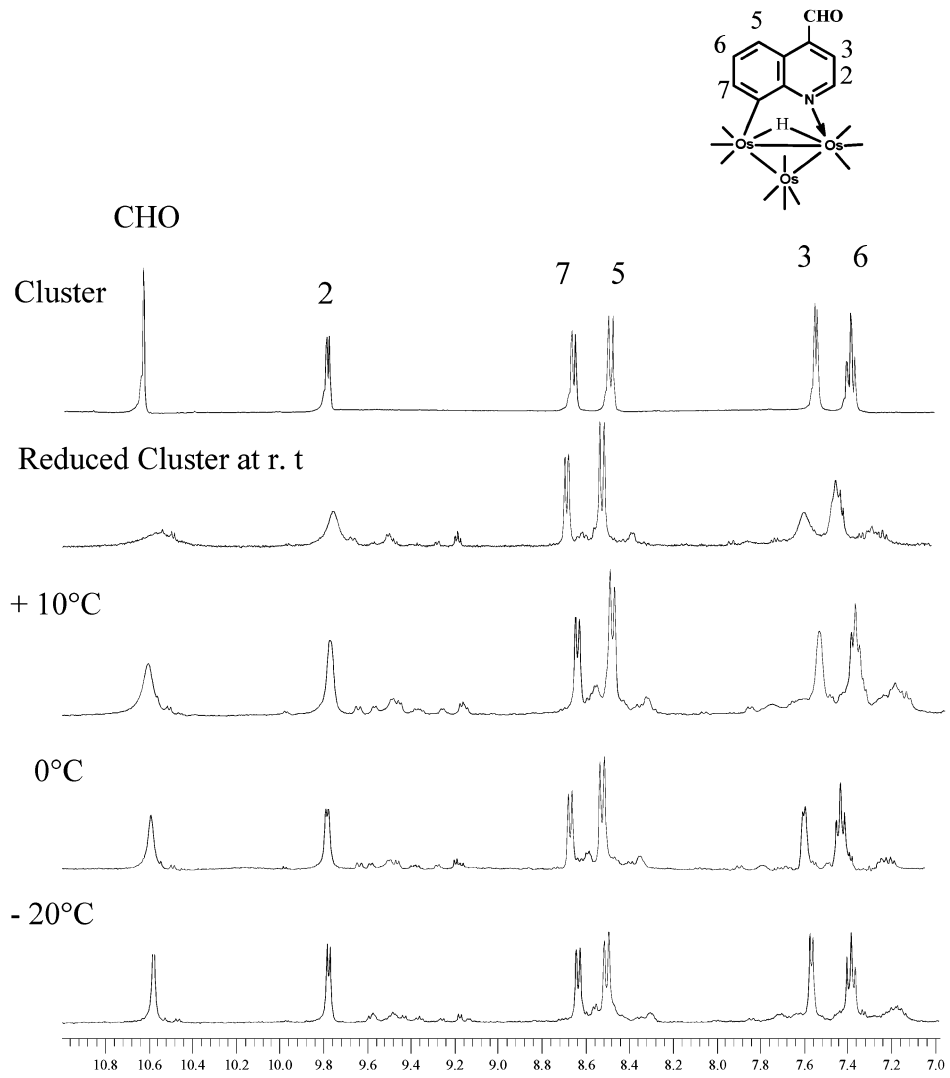

Figure 4. Variable-temperature ^{1}H NMR at 400 MHz of the aromatic region of **4** after addition of cobaltocene.

expected for complete reduction to a diamagnetic dianion and as predicted from the equilibrium constant given in Table 2. Clusters **4** and **6** are partially reduced with cobaltocene and show selective line broadening in their ^{1}H NMR spectra at H(2), H(3), and the aldehyde proton for **4** (Figure 4) and at H(3) and the aldehyde proton for **6**. Addition of excess cobaltocene to **6** triggers decomposition, as evidenced by the appearance of new resonances in the aromatic region. We observe sharpening of the resonances with decreasing temperature for partially reduced **4** (Figure 4). At −20 °C the electron exchange between the reduced/unreduced clusters and also the cobaltocene/cobaltocenium is apparently slow on the NMR time scale. This could be due to the precipitation of the reduced species at that temperature. At room temperature the line broadening in the NMR of **4** is due to the electron-transfer reaction between the reduced and unreduced clusters and also between the cobaltocene and cobaltocenium, as evidenced by the line broadening in the aromatic resonances of **4** and by the observation of one average signal for the cyclopentadienyl protons. This spectroscopic behavior can be understood according to the theory developed by De Boer and MacLean.[22] The electron contribution to the line width (ΔT_{2ex}^{-1}) is given by the equation

$$\Delta T_{2ex}^{-1} = [f_p \tau_p a^2/4]/[1 + f_D \tau^2{}_p a^2/4 + 2\tau_p T_{1e}^{-1}] \quad (1)$$

where τ_p is the lifetime of the paramagnetic molecule, f_p and f_D are the mole fractions of the paramagnetic and diamagnetic molecules, respectively, a is the hyperfine coupling constant, and T_{1e} is the longitudinal relaxation of the electrons. If we assume that the equilibrium constant does not change significantly over the temperature range −20 to +20 °C, the line width will depend only on the rate of exchange and the hyperfine coupling constant for a given resonance. We can therefore, estimate the activation energy by using the relationship

$$\ln \Delta\nu_{1/2} = \ln A - E_a/RT \quad (2)$$

where $\Delta\nu_{1/2}$ is the change in half-height width relative to −20 °C, A is a constant, and E_a is the Arrhenius activation energy. The aldehyde resonance of **4** provides measurable line widths at four temperatures (−20, 0, 10, and 20 °C; Figure 4), and a plot of ln $\Delta\nu_{1/2}$ vs $1/T$ gives a straight line with a correlation coefficient of 0.993 (Figure 5), providing an estimate of $E_a = 11.6$ kcal/mol, which is much higher than for **1** and **2**.[19]

(22) Boer, D. E.; MacLean, C. *J. Chem. Phys.* **1966**, *44*, 1334.

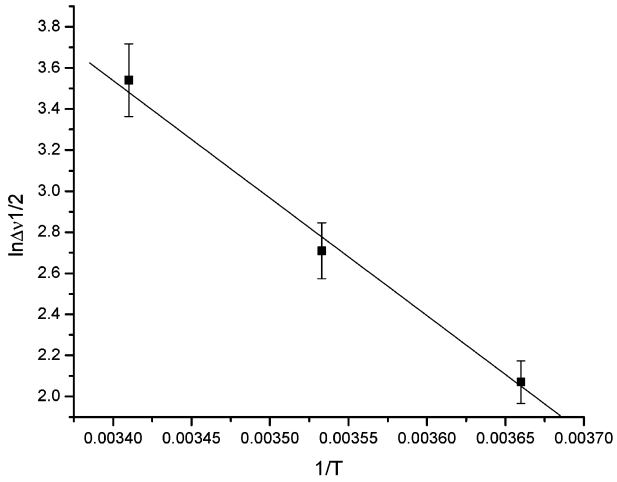

Figure 5. Plot of ln $\Delta\nu_{1/2}$ versus $1/T$ for the aldehyde resonance of partially reduced **4**.

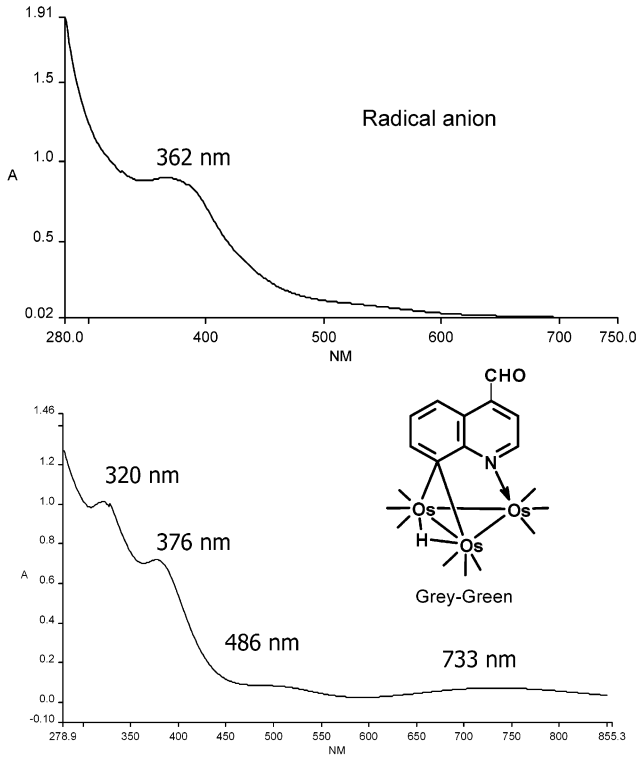

Figure 6. UV−visible spectra of (bottom) **5** and (top) $\mathbf{5}^-$ in CH_2Cl_2.

Upon reduction, the UV−vis spectra of **5** and **4** show disappearance of all the longer wavelength bands (Figure 6). Only absorptions at 362 and 365 nm are observed for the reduced **5** and **4**, respectively. The absorbance around 360 nm could be due to the overlapping absorbances of $CoCp_2$, $CoCp_2^+$, and the reduced clusters.

D. Correlation of the Spectroscopic Data with the Density Functional Theory Calculations. Density functional theory was chosen over other molecular orbital calculation methods, as it provides energy and molecular orbital simulations in less time than other methods.[23] It also takes into account electron correlation, which is very important for calculations involving heavy transition metals.

The density functional theory (DFT) calculations revealed that, for all the clusters, the highest occupied molecular orbital (HOMO) is completely metal based whereas the lowest unoccupied molecular orbital (LUMO) is partly metal and partly ligand based for the electron-deficient clusters **5** and **7** (Figure 7) and for the previously reported **1** and **2**.[19] The LUMO is ligand based for the electron-precise clusters **4** and **6** (Figure 8). For the electron-deficient clusters, the LUMO is primarily composed of 60−70% ligand group orbitals and 30−40% metal orbital contributions. When the LUMO of **5** is plotted on an electron density isosurface (0.05 e/au^3), it is revealed that the most exposed region is on the bond where the aldehyde carbon is attached to the heterocyclic ring, with the remainder of the exposed areas distributed over both rings of the heterocycle (Figure 7). This suggests that the first electron has its density located primarily in the aldehyde group, with the rest delocalized throughout the ring. The spectroscopic evidence indicates that the second electron is impacting the aldehyde carbon as well and goes into the same MO to give a diamagnetic species. On the other hand, for compounds **4** and **6**, the LUMO is mainly on the aldehyde carbon and on the nitrogen-containing heterocyclic ring. In the case of isomeric **4** and **6**, the DFT calculations also reveal that there is a significant difference in their HOMO−LUMO energy gap, which is responsible for the relative reduction potentials and the stability of the resulting radical anion for these two species (Figure 8). A very similar behavior was reported for the cluster $HOs_3(CO)_9(L)$ (L = ortho-metalated α-diimine ligand) by Nijhoff et al.[24] The trend in potential differences and the stability of the resulting radical anion from those clusters is also related to a low-energy LUMO of the clusters, possessing a dominant contribution from the lowest unoccupied π^* orbital of the ligand. The line broadening at the aldehyde H(2) and H(3) resonances in the ^{1}H NMR of **4** is also in agreement with the distribution of calculated spin densities (Figure 9). Thus, the electron-deficient **5** gives a more delocalized radical anion by involving the carbocyclic ring and to some extent the metal core in the MO occupied by the added electron.

Comparing the LUMO's of the electron-deficient isomeric clusters **5** and **7** suggests a rationale as to why **5** showed reversible reduction whereas **7** did not. In the case of **5**, the carboxaldehyde group plays an important role in the formation of the LUMO, whereas in **7**, it is not involved at all, probably as a result of the position of the substituent group. The DFT calculations also reveal that the LUMO of **7** is 14 kcal/mol higher in energy than the LUMO of **5**. Even though the reduction potential for cluster **7** is relatively low (−1.278 V vs $FeCp_2/FeCp_2^+$), the higher LUMO energy and the lack of involvement of the aldehyde group in the LUMO limits the degree of delocalization of the free spin density.

In addition, the LUMO of the free ligand quinoline-3-carboxaldehyde is higher in energy (∼8 kcal/mol) than the LUMO of quinoline-4-carboxaldehyde (Figure 10). Here again, the DFT calculations rationalize the electrochemical behavior of the two heterocycles.

(23) Turki, M.; Daniel, C.; Zalis, S.; Vlcek, A.; Slageren, J. V.; Stufkens, D. J. *J. Am. Chem. Soc.* **2001**, *123*, 11431.

(24) Nijhoff, J.; Hartl, F.; Outersterp, V. J. W. M.; Stufkens, D. J.; Calhorda, M. J.; Veiros, L. F. *J. Organomet. Chem.* **1999**, *573*, 121.

No	HOMO	LUMO	LUMO superimposed onto an electron density isosurface (0.05e/au^3)
5	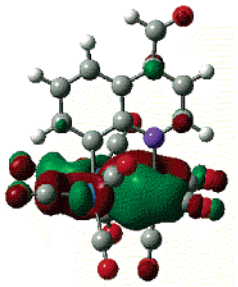	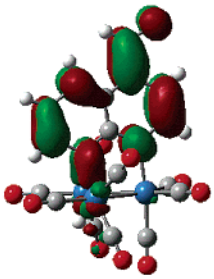	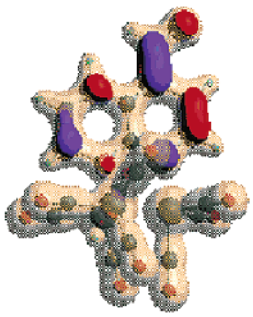 E= -96 kcal/mol
7	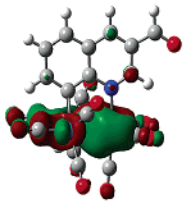	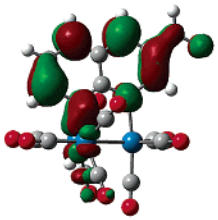	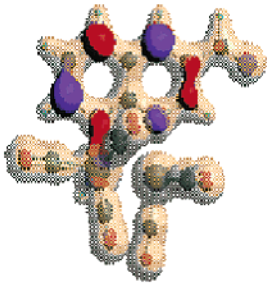 E= -82 kcal/mol

Figure 7. LUMO pictures of **5** and **7** superimposed on an electron density isosurface of 0.05 e/au^3.

Compound	HOMO (isosurface=0.05e/au^3)	LUMO superimposed onto an electron density isosurface (0.05e/au^3)
4	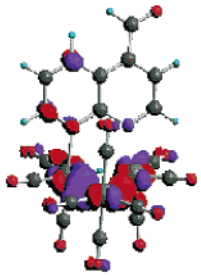 E=-146.07 kcal/mol	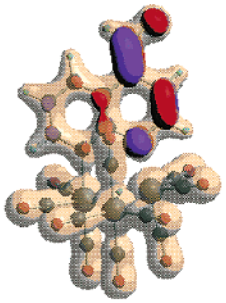 E= -85 kcal/mol
6	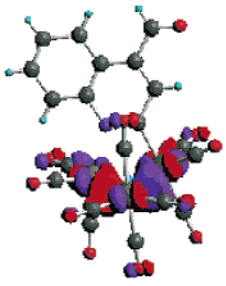 E=-139.6 kcal/mol	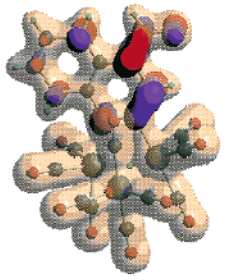 E= -62.6 kcal/mol

Figure 8. LUMO pictures of **4** and **6** superimposed on an electron density isosurface of 0.05 e/au^3.

Experimental Section

Materials and General Procedures. All reactions were carried out under an atmosphere of nitrogen but were worked up in air. Methylene chloride and acetonitrile were distilled from calcium hydride. Methylene chloride-d_2 was purchased from Cambridge Isotope Laboratories and dried over activated

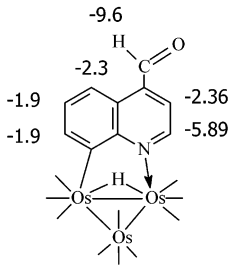

Figure 9. Scaled distribution of unpaired spin density in **4.** The numbers shown are the unpaired spin densities multiplied by 10^3. The sum of all the numbers divided by 10^3 is 1 electron.

molecular sieves. Tetrahydrofuran was distilled from sodium and benzophenone ketyl prior to use. $Os_3(CO)_{12}$ was purchased from Strem Chemicals, used as received, and converted to $Os_3(CO)_{10}(CH_3CN)_2$ by the published procedure.[25] Quinoline-3-carboxaldehyde and -4-carboxaldehyde and tetrabutylammonium hexafluorophosphate were purchased from Aldrich Chemicals and used as received.

Infrared, UV/vis, and ^{1}H NMR spectra were recorded on Thermo Nicolet 633 FT-IR, Perkin-Elmer Lambda 11, and Varian Unity Plus 400 MHz instruments, respectively. EPR spectra were recorded on a Bruker 200 EPR spectrometer equipped with a Bruker ER 031M gauss meter and a HP 5350A microwave frequency counter. Elemental analyses were performed by Schwarzkopf Microanalytical Laboratories, Woodside, NY. Chemical shifts are reported downfield relative to tetramethylsilane.

Synthesis of $Os_3(CO)_9(\mu_3\text{-}\eta^2\text{-L-H})(\mu\text{-H})$ (L = Quinoline-3-carboxaldehyde and -4-carboxaldehyde). $Os_3(CO)_{10}(CH_3CN)_2$ (0.500 g, 0.54 mmol) was dissolved in 200−250 mL of CH_2Cl_2, and a 2-fold molar excess of ligand was added. The reaction mixture was stirred for about 18−20 h and then filtered through a short silica gel column to remove excess ligand. The solvent was removed by rotary evaporation, and the crude product was dissolved in a minimum amount of CH_2Cl_2 and fractionated on silica gel TLC plates using CH_2Cl_2/hexane (30−40% CH_2Cl_2) as the eluent. Two compounds are isolated from the quinoline-4-carboxaldehyde reaction by preparative TLC; the fastest moving orange band is the N−C(2) activated decacarbonyl **6**, whereas the slowest moving red band is the N−C(8) activated cluster **4**. In the case of quinoline-3-carboxaldehyde, we also found two bands, the N−C(8) activated orange-yellow cluster $[Os_3(CO)_{10}(\mu\text{-}\eta^2\text{-L-H})(\mu\text{-H})]$ (**8**; L = quinoline-3-carboxaldehyde), the precursor of **4,** and the N−C(2) activated yellow cluster **9**. Photolysis of **4** and **8** resulted in a brown solution of **5** and a green solution of **7**. The compounds were purified on silica gel TLC plates using CH_2Cl_2/hexane (30−40% CH_2Cl_2) as the eluent. Two bands were eluted. The faster moving orange-yellow (for quinoline-3-carboxaldehyde) and red (for quinoline-4-carboxaldehyde) bands contained minor amounts of **8** and **4**, and the slower moving green (for quinoline-3-carboxaldehyde) and brown (for quinoline-4-carboxaldehyde) bands are the electron-deficient clusters **7** and **5**. These clusters were extracted from the silica using CH_2Cl_2, and the resulting solutions were concentrated to 2−3 mL by rotary evaporation and crystallized from CH_2Cl_2 and hexane at 0 °C. The total yields (based on $Os_3(CO)_{12}$) of the products are given below with the analytical and spectroscopic data.

Compound **4**: Anal. Calcd for $Os_3C_{20}NO_{11}H_7$: C, 23.83; N, 1.38; H, 0.69. Found: C, 23.81; N, 1.28; H, 0.40. IR (ν(CO)) in KBr: 2049 s, 2024 s, 1994 s cm^{-1}. UV/vis in CH_2Cl_2 (λ_{max}): 380, 518 nm. ^{1}H NMR in CD_2Cl_2: δ 10.60 (s, 1H, CHO), 9.76 (d, 1H, H(2)), 8.66 (d, 1H, H(7)), 8.47 (d, 1H, H(5)), 7.54 (d, 1H, H(3)), 7.37 (t, 1H, H(6)) and −12.43 (s, hydride). Yield for **4**: 33%.

Compound **5**: Anal. Calcd for $Os_3C_{19}NO_{10}H_7$: C, 23.29; N, 1.42; H, 0.71. Found: C, 23.11; N, 1.41; H, 0.55. IR (ν(CO)) in KBr: 2076 s, 2046 s, 2018 s, 1980 s, 1947 s, 1982 m, 1710 w cm^{-1}. UV/vis in CH_2Cl_2 (λ_{max}): 320, 376, 486, 733 nm. ^{1}H NMR in CD_2Cl_2: δ 10.34 (s, 1H, CHO), 9.66 (m, 2H, H(2) & H(5)), 8.73 (d, 1H, H(7)), 7.51 (d, 1H, H(3)), 7.38 (dd, 1H, H(6)), −12.23 (s, hydride). Yield for **5**: 31%.

Compound **6**: Anal. Calcd for $Os_3C_{20}NO_{11}H_7$: C, 23.83; N, 1.38; H, 0.69. Found: C, 24.20; N, 1.32; H, 0.89. IR (ν(CO)) in KBr: 2050 s, 2026 s, 2010 s, 2000 m, 1991 m, 1981 m, 1962 w, 1708 w, br cm^{-1}. UV/vis in CH_2Cl_2 (λ_{max}): 334, 448 nm. ^{1}H NMR in CD_2Cl_2: δ 10.33 (s, 1H, CHO), 8.91 (d, 1H, H(5)), 7.94 (m, 2H, H(7) & H(8)), 7.70 (s, 1H, H(3)), 7.63 (m, 1H, H(6)), −14.17 (s, hydride). Yield for **6**: 12%.

Compound	HOMO superimposed onto an electron density isosurface (0.05e/au^3)	LUMO superimposed onto an electron density isosurface (0.05e/au^3)
Quinoline-4-carboxaldehyde	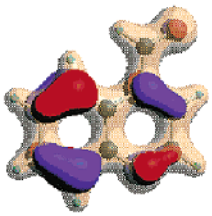	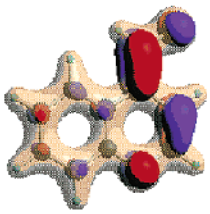 E= -67.6 kcal/mol
Quinoline-3-carboxaldehyde	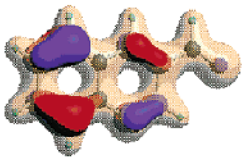	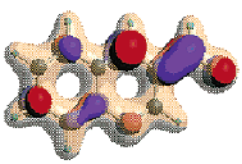 E= -60 kcal/mol

Figure 10. LUMO pictures of quinoline-3-carboxaldehyde and -4-carboxaldehyde ligands.

Compound **7**: Anal. Calcd for $Os_3C_{19}NO_{10}H_7$: C, 23.29; N, 1.43; H, 0.71. Found: C, 23.29; N, 1.33; H, 0.50. IR (ν(CO)) in CH_2Cl_2: 2078 m, 2050 s, 2022 s, 1991 s, br, 1955 w, br, 1943 w, br, 1710 w cm^{-1}. UV/vis in CH_2Cl_2 (λ_{max}): 333, 692 nm. ^1H NMR in CD_2Cl_2: δ 10.08 (s, 1H, CHO), 9.66 (s, 1H, H(2)), 8.70 (d, 1H, H(7)), 8.53 (d, 1H, H(5)), 8.51 (s, 1H, H(4)), −12.06 (s, hydride). Yield for **7**: 30%.

Electrochemistry. Electrochemical measurements were performed with a BAS CV-50W analyzer equipped with a standard three-electrode cell. This cell was designed to allow the tip of the reference electrode to approach closely to the working electrode. Voltammetric experiments were performed using a standard calomel electrode (SCE) as the reference electrode, a glossy-carbon or platinum wire as the working electrode, and a platinum wire as the auxiliary electrode. Potential data are referred to the ferrocene(0/+) couple,[26] which is oxidized in methylene chloride at +0.46 V vs SCE. Typically, a solution containing 1 mM of the cluster and 0.1 M supporting electrolyte (tetrabutylammonium haxafluorophosphate, Bu_4NPF_6) was prepared using freshly distilled and degassed dichloromethane. Positive-feedback *iR* compensation was routinely applied. Polarography was performed with a dropping mercury electrode using a drop time of 1 s.

Preparation of the NMR, IR, UV/vis, and EPR Solutions. Chemical reductions were done in CD_2Cl_2 for NMR studies. Solvents were dried over molecular sieves and degassed prior to use. Samples were prepared in an inert-atmosphere glovebox. Clusters were vacuum-dried to remove surface water before use. Approximately 10 mg (0.01 mmol) of the cluster was dissolved in CD_2Cl_2 in an NMR tube, and then an equimolar amount of a cobaltocene solution (from a 26 mM stock solution) was added to the NMR tube. NMR spectra were recorded within 10−15 min.

For IR and UV/vis spectra we used distilled and degassed CH_2Cl_2. A sodium chloride (permanently sealed 0.10 mm path length) cell was used for IR measurements. The IR sample chamber was purged with nitrogen gas for 2 h before recording the spectrum. The UV/vis spectra were recorded in a screw-cap quartz spectrophotometer cell with a 10 mm path length.

Computational Details

Density functional theory (DFT) calculations were performed using the Gaussian 98 program.[27] The molecular structures from single-crystal X-ray structure determinations were used for geometry optimization. The crystal structure of **4** could not be obtained due to the light sensitivity of the cluster. In the case of **4**, we modified the crystal structure of **3** and used it for the DFT calculations.[28] We used the restricted Becke three-parameter hybrid functional[29] and the Lee−Yang−Parr gradient-corrected correlation function (B3LYP) throughout.[30] The basis sets employed were LanL2dz for the osmium atoms, using the relativistic effective core potential (ECP), which replaces the inner core electrons, and 6-31++G (2d) for the other atoms in all the calculations, except for geometry optimization. No symmetry restrictions were placed on the optimizations. The geometry optimizations were performed on the Os atoms using the same basis set, whereas for the other atoms we used a 3-21G basis set. Geometry optimizations using extended basis sets exceeded our computational capabilities.

Acknowledgment. We gratefully acknowledge the NATO Science Program, the Italian MURST, and the Department of Energy (DOE EPSCoR) for support of this research. We also acknowledge the NIH BRIN program for a faculty travel award (E.R.) and the COBRE Core Computational Facility at the University of Montana.

OM030564M

(25) Lewis, J.; Dyson, P. J.; Alexander, B. J.; Johnson, B. F. G.; Martin, C. M.; Nairn, J. G. M.; Parsini, J. *J. Chem. Soc., Dalton Trans.* **1993**, 981.

(26) Geiger, W. E. *Organometallic Radical Processes*; Elsevier: Amsterdam, 1990.

(27) Closson, W. D.; Wriede, P.; Bank, S. *J. Am. Chem. Soc.* **1966**, *88*, 8.

(28) Rosenberg, E.; Rokhsana, D.; Hardcastle, K. I. Manuscript in preparation.

(29) Becke, A. D. *J. Chem. Phys.* **1993**, *98*, 5648.

(30) Lee, C.; Yang, W.; Parr, R. G. *Condens. Matter* **1988**, *37*, 785.